Global Biogeochemical Cycles

RESEARCH ARTICLE
10.1029/2020GB006622

Linking a Latitudinal Gradient in Ocean Hydrography and Elemental Stoichiometry in the Eastern Pacific Ocean

Jenna A. Lee[1,2], Catherine A. Garcia[1,3], Alyse A. Larkin[1], Brendan R. Carter[4,5], and Adam C. Martiny[1,6]

[1]Department of Earth System Science, University of California, Irvine, CA, USA, [2]Now at Department of Geosciences, Princeton University, Princeton, NJ, USA, [3]Now at Department of Oceanography, University of Hawaii at Manoa, Honolulu, HI, USA, [4]Joint Institute for the Study of the Atmosphere and Ocean, University of Washington, Seattle, WA, USA, [5]Pacific Marine Environmental Laboratory, National Oceanic and Atmospheric Administration, Seattle, WA, USA, [6]Department of Ecology and Evolution, University of California, Irvine, CA, USA

J. A. Lee and C. A. Garcia contributed equally to this work.

Key Points:

- Particulate elemental ratios revealed latitude and biome-specific deviations from Redfield proportions
- We hypothesize nitrogen-limitation leads to elevated Carbon:Nitrogen and Carbon:Phosphorus in the South Pacific Ocean subtropical gyre
- Large size-class particulate ratios (C:N, C:P, N:P) were significantly lower than small size-class ratios, though both decreased poleward in the Southern Ocean

Supporting Information:

Supporting Information may be found in the online version of this article.

Correspondence to:

A. Martiny,
amartiny@uci.edu

Citation:

Lee, J. A., Garcia, C. A., Larkin, A. A., Carter, B. R., & Martiny, A. C. (2021). Linking a latitudinal gradient in ocean hydrography and elemental stoichiometry in the eastern Pacific Ocean. *Global Biogeochemical Cycles*, *35*, e2020GB006622. https://doi.org/10.1029/2020GB006622

Received 1 APR 2020
Accepted 2 MAR 2021

Abstract A past global synthesis of marine particulate organic matter (POM) suggested latitudinal variation in the ratio of surface carbon (C): nitrogen (N): phosphorus (P). However, this synthesis relied on compiled datasets that may have biased the observed pattern. To demonstrate latitudinal shifts in surface C:N:P, we combined hydrographic and POM observations from 28°N to 69°S in the eastern Pacific Ocean (GO-SHIP line P18). Both POM concentrations and ratios displayed distinct biome-associated changes. Surface POM concentrations were relatively low in the North Pacific subtropical gyre, increased through the Equatorial Pacific, were lowest in the South Pacific subtropical gyre, and increased through the Southern Ocean. Stoichiometric elemental ratios were systematically above Redfield proportions in warmer regions. However, C:P and N:P gradually decreased across the Southern Ocean despite an abundance of macro-nutrients. Here, a size-fraction analysis of POM linked increases in the proportion of large plankton to declining ratios. Subsurface N* values support the hypothesis that accumulated remineralization products of low C:P and N:P exported POM helps maintain the Redfield Ratio of deep nutrients. We finally evaluated stoichiometric models against observations to assess predictive accuracy. We attributed the failure of all models to their inability to capture shifts in the specific nature of nutrient limitation. Our results point to more complex linkages between multinutrient limitation and cellular resource allocation than currently parameterized in models. These results suggest a greater importance of understanding the interaction between the type of nutrient limitation and plankton diversity for predicting the global variation in surface C:N:P.

Plain Language Summary Compiled observations of particulate organic matter elemental ratios indicate conservation of N and P where nutrients are scarce, and vice versa in nutrient-rich upwelling and polar regions. However, because the compiled datasets vary in methodology, meso-scale trends are unable to be resolved. In the current study, we observe strong gradients in particulate organic matter (POM) C:N:P ratios using consistent methods for a latitudinal transect in the eastern Pacific Ocean. Single environmental factors were unable to predict variation in C:N:P across regions suggesting a more complex regulation. Ratios of C:N and C:P in the South Pacific Subtropical Gyre were unexpectedly high for a subtropical gyre in the southern hemisphere. A single-nutrient model (nitrate or phosphate) produced significant regional biases, leading us to hypothesize multiple-nutrient models as necessary under conditions of severe nutrient stress. In the Southern Ocean, we measured total and small size fractions to estimate significantly lower C:N:P ratios of larger POM. The N:P ratio of large POM are nearest to the N:P ratio of exported organic matter estimated from remineralized nutrients in the subsurface. This analysis will help evaluate the regional importance of temperatures, nutrient availability, and community structure on biogeochemical cycling.

1. Introduction

The Redfield Ratio (106 Carbon: 16 Nitrogen: 1 Phosphorus) is the widely accepted average proportion of atomic C:N:P of phytoplankton and sinking flux of organic material (Redfield, 1934). Mixing of

remineralized dissolved inorganic nutrients (DIC:DIN:DIP) helps maintain global average proportions, but a variable particulate C:N:P yields a better estimate of deep ocean nutrient concentrations (Devries & Deutsch, 2014; Teng et al., 2014). Global observations of particulate organic matter (POM) suggest latitudinal shifts in POM stoichiometry (Martiny, Pham, et al., 2013). However, these initial observations come from a compilation of 23 datasets applying different analytical methods. A consistent latitudinal quantification of C:N:P can lead to improved understanding and predictions regarding how changes to plankton elemental allocation will affect marine biogeochemical cycles.

In the surface ocean, three main proposed factors affecting C:N:P are nutrient availability, temperature, and community composition (Moreno & Martiny, 2018). N-limitation causes lower-than-Redfield N:P and P-limitation causes higher N:P (Geider & La Roche, 2002; Klausmeier et al., 2004). Micronutrients also play a role in C:N:P variation—the availability of iron could impact phytoplanktons' ability to perform nitrogen fixation and increased N availability (Berman-Frank et al., 2001; Garcia et al., 2020). Higher temperatures increase the efficiency of protein synthesis, requiring phytoplankton to allocate less phosphorus to ribosome production, therefore increasing N:P (Toseland et al., 2013). Lastly, community composition can affect C:N:P via differing life strategies. Allometric differences cause smaller phytoplankton to have a larger cell surface area to volume ratio and increased investments in nitrogen and phosphorus uptake (Finkel et al., 2016; Hein et al., 1995; Klausmeier et al., 2004; Smith & Kalff, 1982). Consequently, small phytoplankton allocate more resources toward N-rich nutrient-acquisition apparatuses (higher N:P), while large, blooming phytoplankton allocate more resources toward a P-rich growth apparatus (lower N:P) (Arrigo, 2005). Additionally, specific groups of phytoplankton have non-Redfield C:N:P or require different nutrients (Arrigo et al., 1999; Baer et al., 2017). Whereas diatoms present in low iron (and high silica) environments can have lower-than-Redfield N:P, diazotrophs can fix nitrogen in high iron environments and drive C:N down and N:P up (Mills & Arrigo, 2010; Price, 2005; Weber & Deutsch, 2010). The combination of all these factors ultimately influences phytoplankton and POM stoichiometry, but the regional variation and importance are still elusive.

Current stoichiometric models that incorporate both the theoretical and observed relationships between differences in environmental conditions generally argue that nutrient availability, particularly phosphate and nitrate, is the primary driver of stoichiometric variability with temperature, light and, community composition playing secondary roles (Galbraith & Martiny, 2015; Pahlow & Oschlies, 2009; Tanioka & Matsumoto, 2017; Teng et al., 2014). However, other papers argue that nutrient availability plays a region-dependent role (Garcia, Baer, et al., 2018; Garcia et al., 2020) and that community composition in, especially the Southern Ocean, can be an important regulator of C:N:P (Arrigo et al., 1999; Weber & Deutsch, 2010). Therefore, multiple environmental and community factors need to be accounted for to create an accurate global model of phytoplankton stoichiometry.

To identify the relationship between C:N:P and various environmental factors, we quantified the stoichiometry of small (<30 μm) particulate organic matter along the GO-SHIP P18 latitudinal transect spanning 28°N to 69°S in the eastern Pacific Ocean, and variation in small and overall particulates south of 54°S. This paper aims to address three questions about variability in elemental stoichiometry: (1) How do variations in the observed data across a strong latitudinal gradient compare to the expected relationship between nutrient availability and C:N:P? (2) How do the observed data compare to the expected relationship between temperature and C:N:P? (3) What effects do different POM size fractions have on C:N:P in the Southern Ocean? We hypothesize that nutrient availability will be the primary driver of C:N:P variability across biomes (Garcia, Baer, et al., 2018), with temperature and community composition playing a secondary role.

2. Materials and Methods

2.1. POM Sample Collection

POM samples were collected along the Global Ocean Ship Based Hydrographic Investigations Program (GO-SHIP) P18 line during a November 2016–February 2017 expedition on the NOAA R/V Ronald H. Brown (more information on the P18 transect in Section 3.1). Samples were collected from the California Current System to the Southern Ocean Polar Front (Table S1).

General equipment preparation in the lab before shipment included an HCl bath (1.0 M HCl overnight) and milli-Q rinse for the 8-L carboys, tubing, and filter holders. Additionally, the filtration equipment above was autoclaved prior to shipment. The 25 mm, 0.7 μm GF/F filters and aluminum foil used to wrap the filters were combusted (500°C for 5 h) in aluminum foil packets to remove any traces of carbon present. The forceps that came in contact with the samples were wiped with 70% ethanol before and between uses.

Seawater for the POM samples was collected from the onboard flow-through underway system. The underway intake was located off the bow of the ship at a depth of approximately 5.3 m from the sea surface and the length of the pipe from the intake location to the output lab was 11.8 m. We interpreted these samples to be representative of the entire mixed layer (under the assumption that the mixed layer is well-mixed) (Figure S1). A 30 μm nylon mesh pre-filter was attached to the underway outlet for all standard "small size-class" samples to remove large plankton and particulates. Before sampling, the carboys used were rinsed twice with the pre-filtered underway seawater. Additional "total POM" samples were taken in the Southern Ocean by removing the 30 μm pre-filter during the rinse and sample collection steps. Triplicate sampling for both particulate organic phosphorus (POP), particulate organic carbon (POC), and particulate organic nitrogen (PON) occurred roughly at four-hour intervals with a shift forward of one hour each day. For example, if samples were taken at 01:00, 05:00, and 09:00 on one day, samples would be taken at 02:00, 06:00, and 10:00 the following day to avoid any diurnal bias. POP was collected separately (different container and filter) than POC/N samples. As POP was collected separately, pooled standard deviations were used for POM C:P and N:P ratios. The water was vacuum filtered through combusted GF/F filters and the volume of seawater filtered was consistent between all POM samples at each station and determined on a per station basis, ranging from 3 to 8 L. The volume was raised if the previous stations' filtration times exhibited a decreasing trend and lowered if filtration time exhibited an increasing trend in an attempt to normalize the amount of collected material. The large sampling volume and initial rinsing steps limit the effect of a time delay from underway inlet to sampling station. After filtration, all POP triplicates were rinsed with approximately 2–5 mL of a 0.17 M Na_2SO_4 solution consistent with Lomas et al. (2010) and Solorzano and Sharp (1980). All POM samples were folded in half with the top sides toward each other, sealed inside pieces of combusted aluminum foil, and stored in a −20°C freezer until analysis.

2.2. POP Assay

The POP data were obtained using an ash/hydrolysis method and comparing the samples to a set of standard phosphorus concentrations (Lomas et al., 2010). The sample filters were unfolded and placed face up into acid-bathed and combusted scintillation vials. Along with each set of samples, 10 different volumes (ranging 0–0.5 mL) of 0.1 M KH_2PO_4 solution were added to scintillation vials. 2 mL of a 0.017 M $MgSO_4$ drying solution was added to each scintillation vial and then all vials were placed into an 80–90°C oven overnight to dry. After drying, the vials were heated at 500°C for 2 h, then left to cool before adding 5 mL of 0.2 M HCl to each vial and being returned to the 80–90°C oven for 30 min after being brought up to temperature. The solutions were then transferred to acid-bathed 15-mL glass centrifuge tubes. The sample vials were rinsed with 5 mL of milliQ each, which was also added to the centrifuge tubes. 1 mL of a mixed reagent containing 2:5:1:2 parts Ammonium Molybdate (CAS: 12054-85-2), 5.0 N H_2SO_4, Potassium Antimonyl Tartrate (CAS: 28300-74-5), and Ascorbic Acid (CAS: 50-81-7) respectively was added to each centrifuge tube in 30-s intervals. Each of the sample tubes was centrifuged to isolate any glass fibers that could interfere with the absorbance reading. Lastly, after allowing the mixed reagent to react for exactly 30 min, the standards and samples were analyzed in 30-s intervals in a spectrophotometer at an 885 nm wavelength using a blank of ~0.1 M HCl solution and rinsing the cuvette with the blank solution between measurements. Detection limit for phosphorus measurements was 0.310 μg.

2.3. POC/PON Assay

POC and PON measurements were analyzed both in-lab at UCI and at the UC Santa Barbara Marine Science Institute Analytical Lab. An ANOVA analysis determined that the two methods did not produce significantly different results (p-value = 0.540 for POC and p-value = 0.531 for PON). The preparation for all samples was the same; the samples were each removed from their foil packets and placed into acid-bathed and combusted scintillation vials and dried in a 55°C oven overnight. The scintillation vials were then

placed in a desiccator containing a beaker of 12 M HCl overnight to minimize inorganic carbon contamination (Ducklow & Dickson, 1994). Lastly, the samples were dried at 55°C at least overnight. Samples sent to UCSB were then capped and shipped to the lab. UCSB's POC and PON measurements had a mean detection limit (DL) of 2.35 ± 0.73 μg and 2.98 ± 1.14 μg respectively. Samples analyzed at UCI were packed into tin packets alongside Atropine (CAS: 51-55-8) standards (ranging 0.2–1.5 mg) and measured using a Flash EA elemental analyzer with a DL of 100 ppm and a carrier flow rate of 130 mL/min. For all model analyses, triplicate averages were used resulting $N = 188$ observations for POC, PON, POP, C:N, C:P, and N:P. All POM data were published in a public repository at BCO-DMO (http://doi.org/10.26008/1912/bco-dmo.816347.1).

2.4. Nutrient Availability, Chemical, and Physical Properties

Hydrographic data described here is available at the Carbon and CLIVAR Hydrographic Data Office website (https://cchdo.ucsd.edu) for bottle and CTD data (Mordy et al., 2017). Underway sea surface temperatures are available on the NOAA National Centers for Environmental Information thermosalinograph data portal website (https://www.nodc.noaa.gov/tsg/). Salinity, temperature, and pressure were measured from the conductivity, temperature, and depth (CTD) rig as it was being lifted up through the water column. Ambient nutrient concentrations (nitrate, phosphate, and silicate) were measured from the rosette Niskin bottles at each GO-SHIP station. Concentrations were measured using the GO-SHIP nutrient protocol for the P18 hydrographic expedition on board the research vessel using an auto-analyzer. Detection limits for Nitrate and Phosphate were 0.1 and 0.01 μM, respectively. Nitrate concentrations often fell below the detection limit and were assumed to be 0.1 μM for use in statistical analysis and model predictions. Environmental factors were tested for significance in linear regression models against POC, PON, POP, C:N, C:P, and N:P using a 1-way ANOVA using MATAB fitlm.m.

The P18 Line was from November 2016 to January 2017 during a week La Niña. To compare the 2015/16 El Niño to the 2016/17 La Niña in the Pacific Ocean, we visually compared environmental conditions tracked by remote sensing. November to January monthly averages were used for precipitation, wind speed/direction, sea surface temperature, and chlorophyll. Precipitation was a merged satellite product from Goddard Earth Sciences Data and Information Services Center at https://disc.gsfc.nasa.gov/datacollection/GPM_3IMERGM_06.html (Huffman et al., 2019). Winds speed/direction NCEP Reanalysis data were provided by the NOAA/OAR/ESRL PSD, Boulder, Colorado, USA, from their Web site at https://www.esrl.noaa.gov/psd/ (Kalnay et al., 1996). Sea surface temperature and chlorophyll were from the NASA Ocean Ecology Laboratory MODIS-Aqua satellite at https://oceandata.sci.gsfc.nasa.gov/ (NASA Ocean Ecology Laboratory).

2.5. Regional Analysis

Biomes were separated using a depth profile of potential density along the P18 transect. Potential density was calculated using the temperature, salinity, and pressure measurements from the CTD sensors. The surface densities (4–20 m depth) were smoothed across stations at each depth with a 21-point moving average and the approximate density gradient between stations was determined for each depth by finding the slope between points. The density gradients were then summed across depths and smoothed across stations with an 11-point moving average. The locations of maximum change were considered to be ocean fronts (Figure S2). The peak locations were averaged and considered a single front if multiple peaks were found within one station of each other. The first three peaks/troughs were ignored due to initial small scale hydrographic variability, as high resolution sampling began at 22.8°N. Distance between stations was unevenly spaced and ranged from 0.05 to 169.16 km with a median distance of 49.2 km. This method yielded nine different biomes: the California current (CAcurr), the northern and southern halves of the North Pacific Gyre (NPgyre_N and NPgyre_S respectively), the equator and equatorial South Pacific (Eq and EqSP), the northern and southern portions of the South Pacific Gyre (SPgyre_N and SPgyre_S), the Subantarctic (SubAnt), and the southernmost region along the sea ice (AntIce).

We also compared C:N:P regional averages according to three other biome definitions to test whether boundary definitions impacted the results. For the "Teng Biomes" the regional boundaries are separated according to 0.3 mmol m^{-3} contour of annual mean PO_4^{3-} concentrations (Teng et al., 2014). P18 passed

through 3 Teng biomes; (1) Equatorial Pacific Ocean (EqPO), (2) South Pacific Subtropical Gyre (SPSG), and (3) Southern Ocean (SO). For the "Fay Biomes," the regional boundaries are determined by sea surface temperature, seasonal chlorophyll a concentrations, ice fraction, and maximum mixed layer depth as described previously (Fay & McKinley, 2014). P18 passed through 6 Fay biomes; (1) North Pacific subtropical permanently stratified (NP-STPS), (2) Eastern Pacific equatorial upwelling (PEQU-E), (3) South Pacific subtropical permanently stratified (SP-STPS), (4) Southern Ocean subtropical seasonally stratified (SO-STSS), (5) Southern Ocean subpolar seasonally stratified biome, and (6) Southern Ocean ice (SO-ICE) biomes. For the "Longhurst Biomes", the biogeochemical provinces were determined by bathymetry, chlorophyll a concentration, surface temperature, and salinity as described previously (Reygondeau et al., 2013). P18 passed through 8 Longhurst Biomes; (1) Central American coast (CAMR), (2) North Pacific equatorial counter current (PNEC), (3) Pacific equatorial divergence (PEQD), (4) South Pacific gyre (SPSG), (5) South subtropical convergence (SSTC), (6) Subantarctic water ring (SANT), (7) Antarctic (ANTA), and (8) Austral polar (APLR). Annual averaged biome definitions were used in each case. Biome average POM ratios and concentrations were tested for regional significance using a 1-way ANOVA, p-value < 0.05 (Tables S2 and S3), and for significance difference from Redfield proportions using a t-test, p-value < 0.05 (Figure S3).

2.6. Model Comparison

We compared the observed ratios of C:N:P to model estimates from several studies. The single-nutrient-only linear models used inputs of ambient PO_4^{3-} concentration for C:P and NO_3^- concentration for C:N (Galbraith & Martiny, 2015). While the C:P to PO_4^{3-} relationship is linear in the source publication, the C:N ratio flattens out at high nitrate concentrations. Thus, the authors chose a linear model for C:P and a hyperbolic model for C:N based on phosphate and nitrate, respectively. The equations used were $\mathrm{C{:}P} = \frac{1}{6.0E^{-3} \times \left[\mathrm{PO_4}\right]^{3-} + 6.0E^{-3}}$ and $\mathrm{C{:}N} = \frac{1}{0.125 + \left(\frac{3.0E^{-3} \times \left[\mathrm{NO_3}\right]^-}{0.32 + \left[\mathrm{NO_3}\right]^-}\right)}$ (where "[ ]" is used to indicate concentrations), and the surface concentrations were used as ambient nutrient concentrations. N:P was calculated based off of the results of the other nutrient-only models; $\mathrm{N{:}P} = \frac{\text{nutrient} - \text{only predicted POC:P}}{\text{nutrient} - \text{only predicted POC:N}}$. The regression slope and intercept for the Galbraith Martiny P:C model was refit using P18 data only with fitlm.m in MATLAB. For C:N, the hyperbolic model coefficients were refit using fitnlm.m.

The temperature-only linear models for C:P and N:P used sea surface temperature as input (Yvon-Durocher et al., 2015). The equations used were $\mathrm{C{:}P} = e^{3.7E-2*(T-15)+5.010}$ and $\mathrm{N{:}P} = e^{3.2E-2*(T-15)+2.909}$. C:N was calculated off of the results of the other temperature-only models; $\mathrm{C{:}N} = \frac{\text{temperature - only predicted POC:P}}{\text{temperature - only predicted PON:P}}$. Internal surface temperature, the temperature at the depth of the underway system, was used as the sea surface temperature equivalent. The regression slopes and intercepts for the Yvon-Durocher ln(C:P) and ln(N:P) models were refit using P18 data only with fitlm.m in MATLAB.

For C:P, the multivariate trait model used inputs of light (photosynthetically active radiation, PAR), PO_4^{3-}, and temperature to determine the optimal ratio at each location (Moreno et al., 2018). PAR values were obtained using 8-day MODIS-Aqua observations with a 9 km resolution (NASA Ocean Biology Processing group; MODIS-Aqua).

2.7. Southern Ocean Analysis

The deviation of nutrient concentrations from the Redfield ratio (N*) was calculated using the equation: $\mathrm{N^*} = \left[\mathrm{NO_3}\right]^- - 16\left[\mathrm{PO_4}\right]^{3-}$ Profiles are interpolated every 1m from the surface to 800m depth using a linear interp1.m in MATLAB. To reduce artifacts between stations, profiles are smoothed across stations with a span of 20%. The rloess method was used to assign lower weight to outliers. ΔN* calculated as difference between mixed layer (0–75 m) and thermocline (200–800 m) averages, respectively, using this interpolated grid.

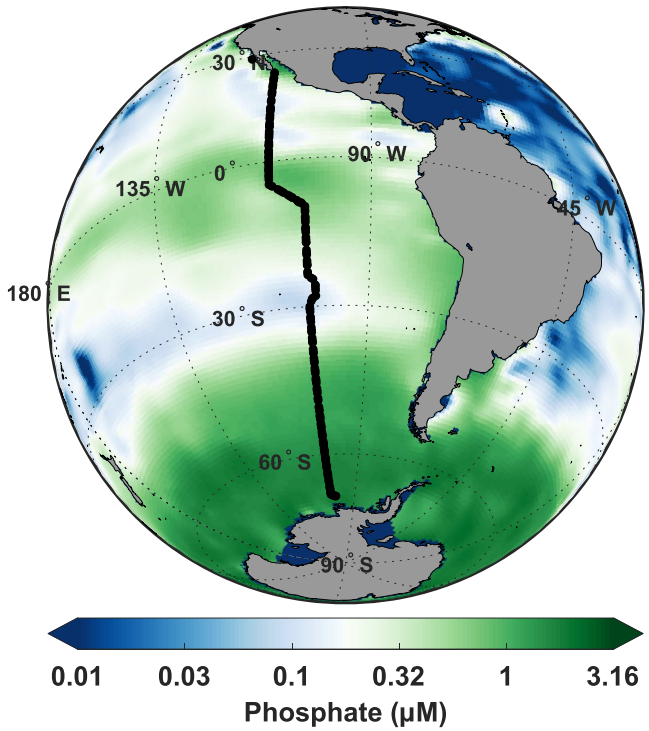

Figure 1. GO-SHIP P18 Cruise transect. The cruise transect with sample locations (black, $n = 188$) superimposed on the climatological phosphate concentration (μM) (Lauvset et al., 2016).

The large POM > 30 μm concentrations were calculated by subtracting the pre-filtered POM concentrations (small POM < 30 μm) from the total concentrations at each station. Any negative concentrations were discarded. After the stoichiometric ratios were calculated, any outlier values (C:P > 500, N:P < 1, N:P > 100) were also discarded (Table S4). Triplicates were averages after outlier omissions. An ANOVA was run between the large and small stoichiometric ratios, and the large and small POM were determined to be statistically different (p-value $< 7 \times 10^{-4}$).

3. Results

3.1. P18 Transect, POM Concentrations, and C:N:P

As part of Bio-GO-SHIP, we collected samples along the P18 line in the eastern Pacific Ocean from the coast of Baja California, Mexico (28°N, 116°W) down to the ice-edge off Antarctica (69°S, 103°W) between November 2016 and January 2017 (Figure 1). The cruise covered four main regions: the North Pacific Subtropical Gyre (NPgyre; 28°N to 5°N), the Equatorial Pacific (EqPac; 5°N to 10°S), the South Pacific subtropical gyre (SPgyre; 10°S to 40°S), and the Southern Ocean (SOcean; 40°S to 69°S), each of which had distinct environmental characteristics (Table S1). The track started close to the Central American coast and continued along the eastern edge of NPgyre. The cruise occurred during a weak La Niña period, therefore, the northern portion of NPgyre experienced slightly higher than average upwelling and nutrient input at the time of the study (Escribano et al., 2004) (Figure S4). Sea-surface temperatures (SST) were highest in NPgyre and ranged from 22.6 to 29.6°C (Figure 2d). The Intertropical Convergence zone (ITCZ) and North Equatorial Counter Current (NECC) were positioned near 7°N, with the Southeast Trade Winds resulting in stronger upwelling southwards (Figure 2, Figure S4). The upwelling region had high silicate concentrations compared to the regions adjacent to it and SST ranged from 21.6 to 26.5°C during the time of data collection (Figures 2c and 2d).

The South Pacific subtropical gyre had low nutrient concentrations and intermediate SSTs ranging from 16.5 to 25.3°C. On average, EqPac exhibited nutrient shoaling (nutricline 11.2 ± 19.3 m), followed by deepening in NPgyre (49.8 ± 22.0 m) and SPgyre (107.6 ± 86.5 m) (Table S1). Lastly, the SOcean had high nutrients but a wide range in SST (0.0–13.6°C). Not only did surface macronutrients approach Redfield proportions relative to other regions ($[NO_3]^-$:$[PO_4]^{3-}$ of 13.5 ± 1.7), but silicate concentrations also increased significantly (SiO_4^{2-} maximum 47.6 μmol kg^{-1}) along P18 in the SOcean.

The POM concentrations varied by biome (as defined broadly in Section 3.1 and in detail in Section 2.5) and both POC and PON showed strong covariance with POP ($R^2 = 0.79$ and $R^2 = 0.84$, respectively, p-value < 0.001) and each other ($R^2 = 0.98$, p-value < 0.001) (Figure 2e, Figure S5, Table S1). POC was low in NPgyre, increased through EqPac with a small peak right at the equator, reached a minimum in SPgyre, and then steadily increased from 30°S through the SOcean with local maxima at 45°S, 52°S, and 70°S. Biome divisions were comparable to published studies based on climatological data (Figure S3). Thus, there was significantly distinct biome variation in POM concentrations (Table S2).

The stoichiometric ratios commonly deviated from Redfield proportions and displayed distinct biome values (Figures 2f–2h, Table S1). Average C:N (6.3 ± 0.6) across the entire transect was close to Redfield proportions (Table S1), but several regions had unique ratios (Figure 3, Figure S5). C:N was significantly higher in the two gyre regions and peaked at 8.3 in the center of SPgyre. In contrast, C:N was mostly below Redfield proportions in EqPac and the SOcean. We found that C:N and C:P were more related when SST was warm (above 20°C), and C:P and N:P when cold. Similar to C:N, C:P exhibited a small peak in NPgyre and a large peak in SPgyr but declined throughout SOcean. N:P showed limited variation in warmer regions although there was a small peak in SPgyre center. C:P and N:P were on average 135 ± 29 and 21.5 ± 3.7, respectively.

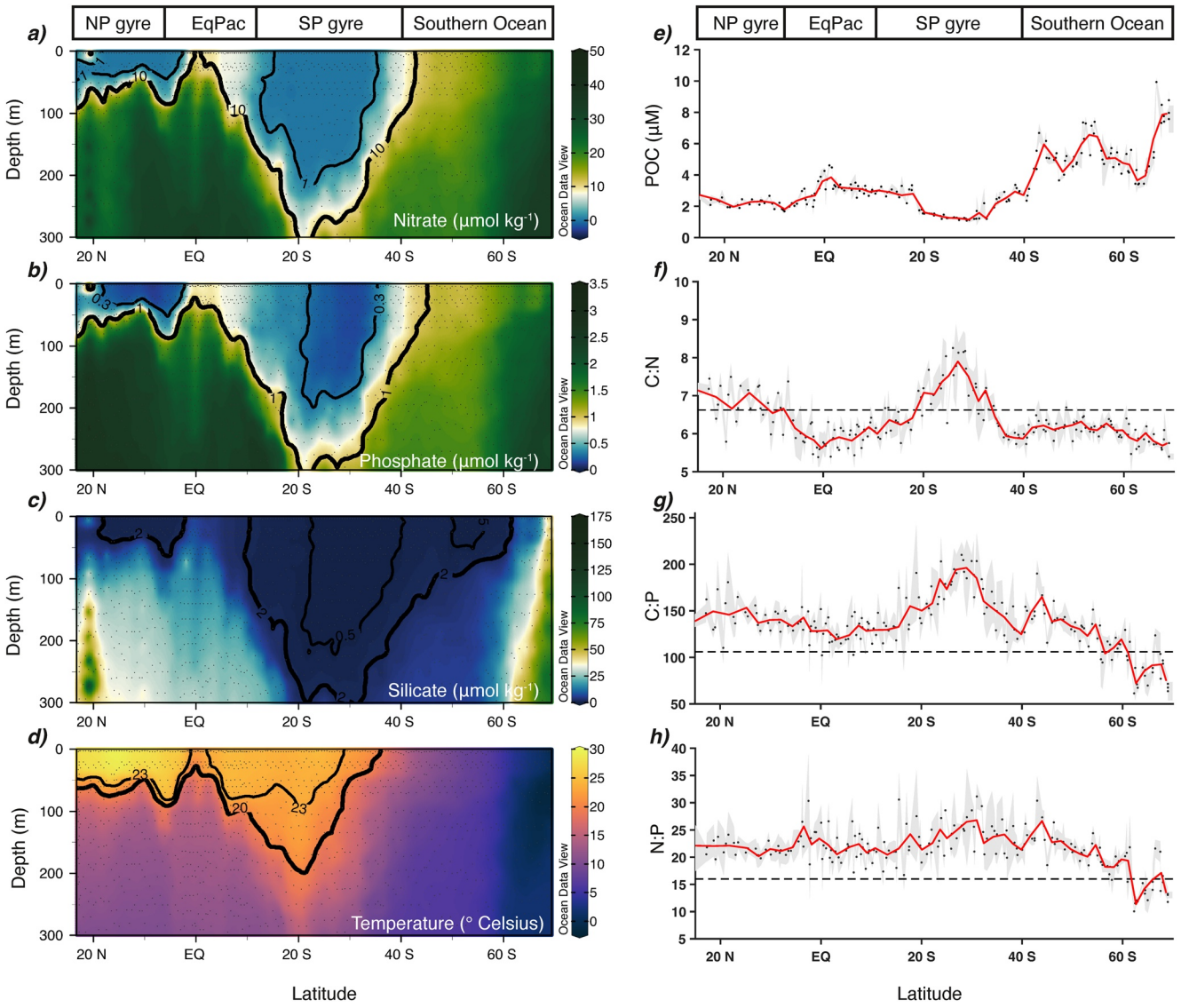

Figure 2. Environmental gradients, POM concentration, and ratios. Observed nutrient and temperature section gradients. (a) Nitrate, (b) phosphate, and (c) silicate concentrations. d) Temperature. Triplicate averaged surface POM concentrations and molar ratios were plotted according to latitude for (e) POC, (f) C:N, (g) C:P, and (h) N:P. The trendlines (red) represent daily averages and the standard deviation (gray shading) are shown behind the data. The black dashed line represents Redfield proportions. POM, particulate organic matter.

Both ratios showed continued declining trends south of SPgyre edge. Thus, we observed clear biome-specific elemental ratios leading to significant latitudinal shifts in C:N:P (Table S3).

3.2. Southern Ocean Size Ratios

Latitudinal shifts in SOcean elemental ratios were linked to particle size-classes and hydrography. In the southern section of SOcean, we estimated POM concentrations and ratios from two different size classes (POM < 30 µm and POM > 30 µm) to test the effect of particle size on POM stoichiometry. The minimum SOcean POC occurred near the maximum of water mass divergence south of the Polar Front (near 62°S along P18 using water property definitions of Orsi et al., 1995). Throughout SOcean, POM > 30 µm accounted for an average of 17% of the total POC and PON concentrations (Figures 4a and 4b). However, POP > 30 µm contributed to 31% of total POP concentration and thus a relatively higher proportion compared to the other elements (Figures 4i and 4c). POM > 30 µm and POM < 30 µm also had statistically

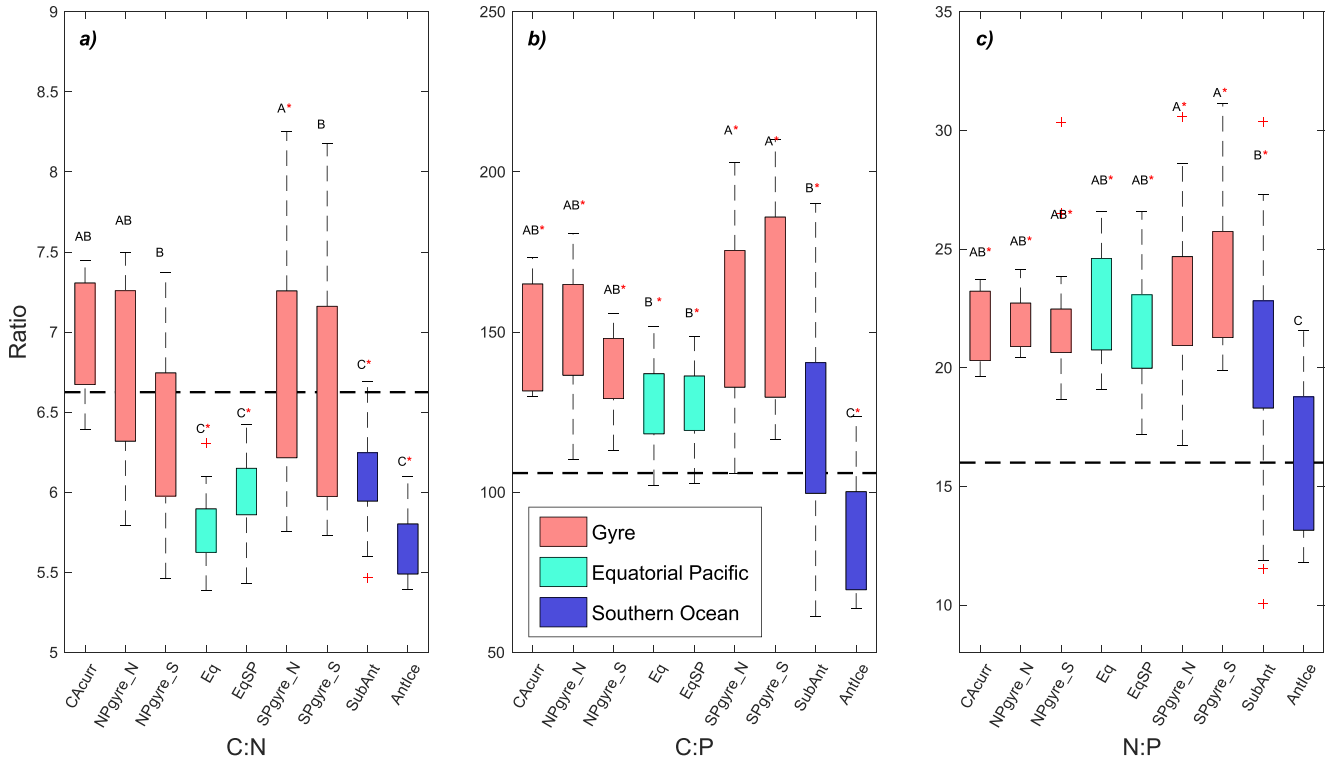

Figure 3. Regional POM stoichiometry. The data were separated by latitude for each of nine regions (as defined in Section 2.5), and represented by boxplots for each of the stoichiometric ratios—(a) C:N, (b) C:P, (c) N:P. The red dashed line represents the Redfield ratio for a given stoichiometric ratio. Significant regional differences are denoted with letters above plot based on Tukey post-hoc honest significant difference test. For all boxplots, a black bar represents the median value. The interquartile range bars are colored by the four Main Biomes (defined in Methods). Outliers are marked with a "+" symbol, and the whiskers mark the range (min, max) of values excluding outliers. The outliers are defined as more (less) than 1.5 times the min (max) of the interquartile range. POM, particulate organic matter.

different stoichiometry (Figures 4g–4k) with consistently depressed C:P, C:N, and N:P ratios within the large size fraction. As the large size fraction contributed larger amounts to the biomass at high latitudes in SOcean, the lower elemental ratios among large particles contributed to a depressed POM_{total} C:N:P.

3.3. Linking Southern Ocean Hydrography and Stoichiometry

We examined the detailed shifts in hydrography and elemental stoichiometry in SOcean to evaluate a series of previously proposed hypotheses regarding the link between plankton nutrient requirement, nutrient supply, and the deep-ocean nutrient pools. Multiple studies have proposed that deep-ocean DIN:DIP ratios are maintained near Redfield values by physical ocean mixing despite non-Redfield proportions in surface plankton communities (Figure 5a) (Martiny, Pham, et al., 2013; Mills & Arrigo, 2010; Weber & Deutsch, 2010). In support, we observed a decrease for surface POM N:P inversely following an increase in surface DIN:DIP (Figure 5c). This provides regional empirical support that a depressed uptake ratio of DIN:DIP of the SOcean surface plankton—assumed to make up most POM—leads to elevated residual DIN:DIP. Furthermore, the southward decrease in surface POM N:P was coupled to the gradient in surface and subsurface N* with positive differences to the north of 54°S and negative to the south (Figures 5c and 5d). More quantitatively, the N* minimum measured between 50 and 100 m depth averaged 2.3 μmol kg^{-1} more N and 0.28 μmol kg^{-1} more P than in the N* maximum just above when considered between the 57.1°S Sub Antarctic Front and the 67.8°S Southern Antarctic Circumpolar Current Front. Assuming similar source waters, this was consistent with a biological pump of organic matter with a N:P ratio of 8.2, very similar to the average large POM > 30 μm N:P ratio of 9.4 over this latitude range. In their model, Weber and Deutsch (2010) showed that the increasing N* in surface waters was driven by preferential phosphorus uptake by the community of faster-growing diatoms. Thus, past modeling efforts and the observed trends

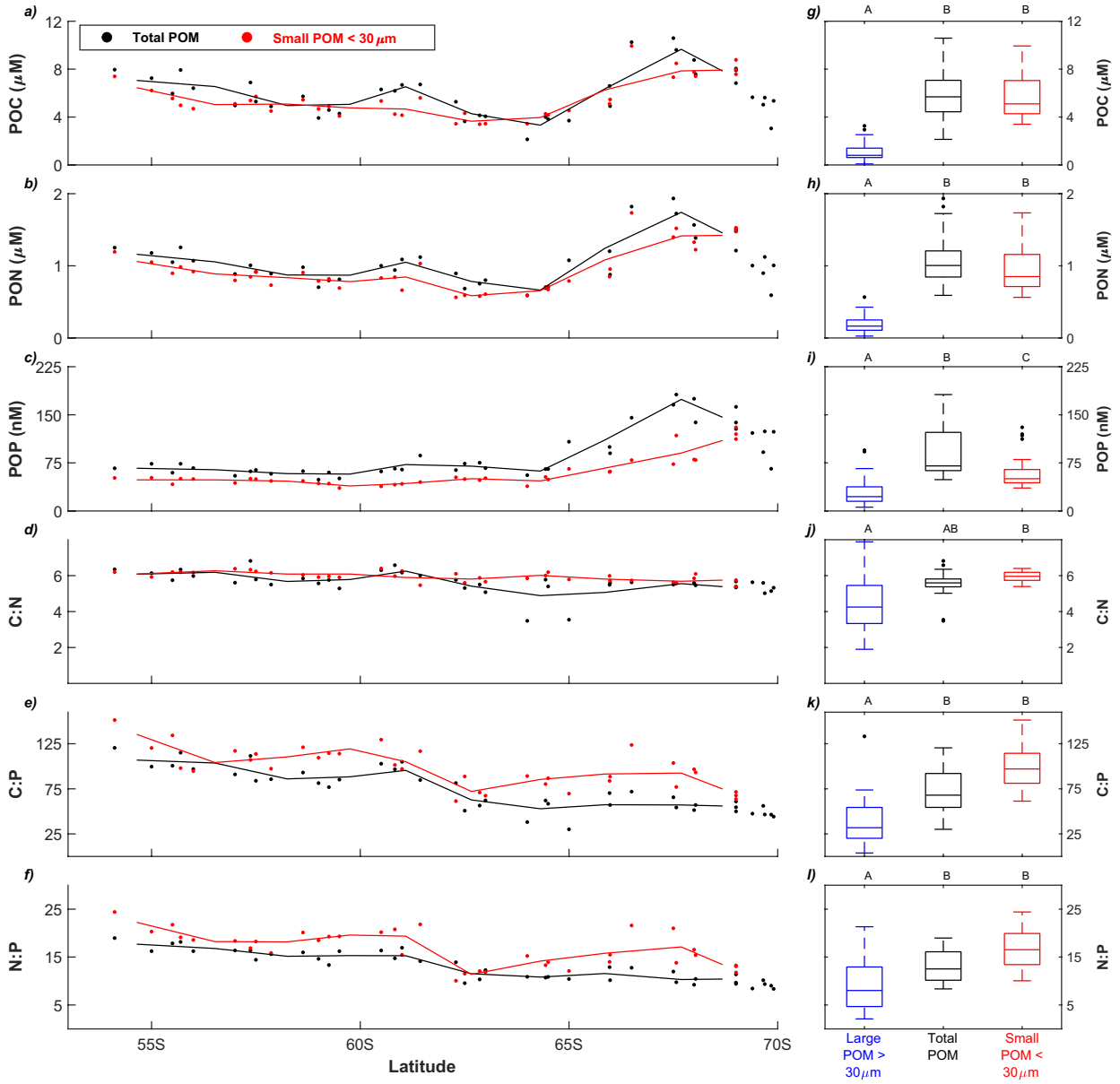

Figure 4. Southern ocean size class POM stoichiometry. The Small (POM ≦ 30 μm, red) and Total (black) POM concentrations and ratios are plotted alongside their respective daily average lines for (a) POC, (b) PON, (c) POP, (d) C:N, (e) C:P, and (f) N:P. Large (POM > 30 μm, blue) is predicted from the difference between Total and Small POM size fractions. Next to each scatterplot is the boxplot for the Large, Total, and Small data—(g) POC, (h) PON, (i) POP, (j) C:N, (k) C:P, and (l) N:P. Significant size fraction differences are denoted with letters above plot based on Tukey post-hoc honest significant difference test. For all boxplots, a black bar represents the median value. The interquartile range bars are the bottom and top of the box. Outliers are marked with a "+" symbol, and the whiskers mark the range (min, max) of values excluding outliers. The outliers are defined as more (less) than 1.5 times the min (max) of the interquartile range. POM, particulate organic matter.

in particulate versus dissolved nutrient ratios support that surface ocean ecological processes can result in significant differences in the dissolved, particulate, and exported nutrient ratios.

3.4. The Relationship Between POM and Environmental Factors

Environmental factors associated with nutrient availability partially explained the regional variations in C:N:P. We ran linear regression models for six environmental factors that are thought to be important for regulating POM elemental stoichiometry (Moreno & Martiny, 2018) (Table S5). Terms associated with

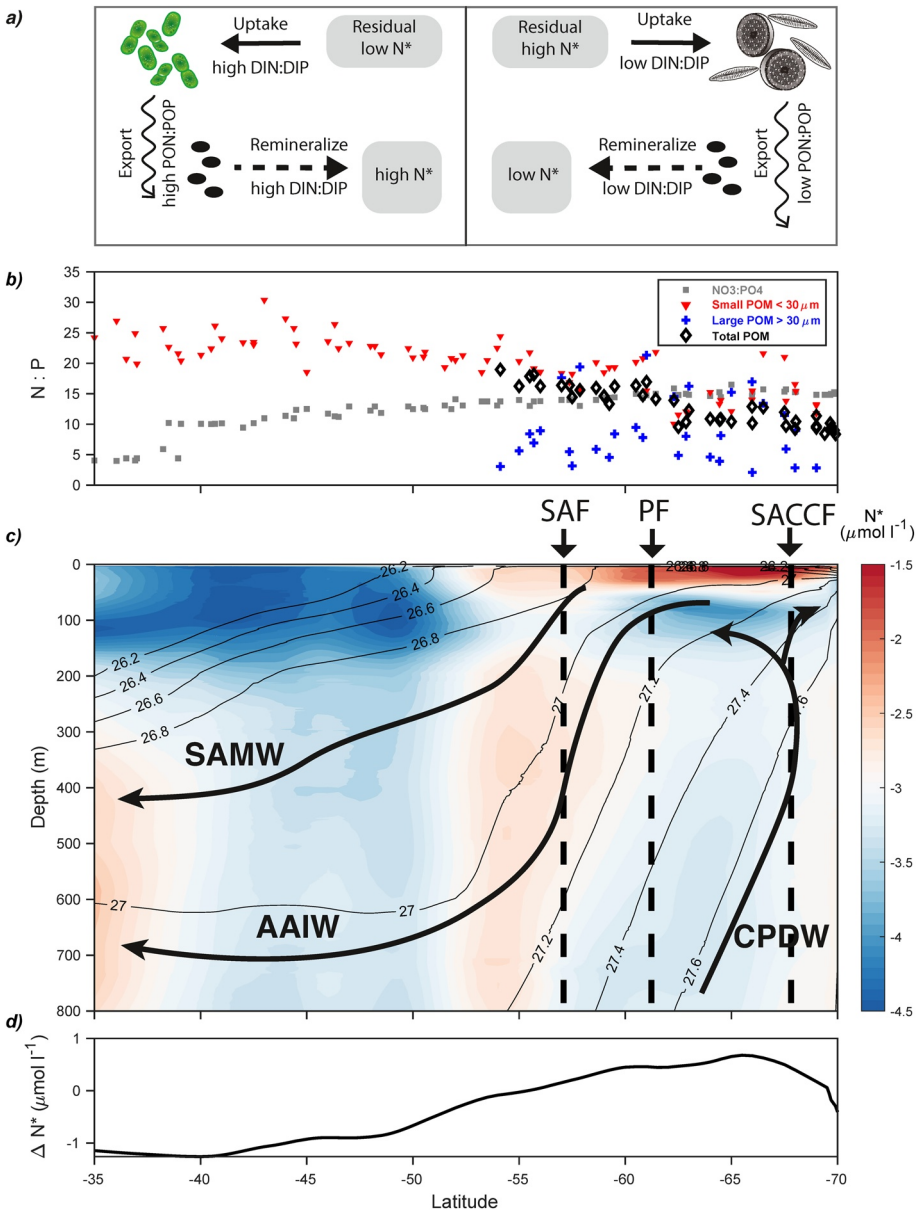

Figure 5. Southern Ocean N*, potential density, and N:P of dissolved and particulate matter. Evidence for biologically mediated circulation averaging hypothesis with: (a) Conceptual diagram of Cyanobacteria- (left) versus diatom- (right) dominated communities and their imprint on N* of surface and thermocline water. (b) Scatter plot of surface N:P of $\left[NO_3\right]^-$:$\left[PO_4\right]^{3-}$ (gray squares), small POM < 30 μm (red triangles), large POM > 30 μm (blue plus), and total POM (black diamonds). (c) Observed N* (N* = $\left[NO_3\right]^-$ −16$\left[PO_4\right]^{3-}$) with potential density contours shown in the top 800 m. (d) ΔN* calculated as difference between mixed layer (0–75 m) and thermocline (200–800 m) averages, respectively. Figure is a recreation of Weber and Deutsch (2010) in Ocean Data View with cmocean color palette. DIN = dissolved inorganic nitrogen. DIP = dissolved inorganic phosphorus. POM = particulate organic matter. POP(N) = particulate organic phosphorus(nitrogen). Water masses are abbreviated as SAMW = Sub-Antarctic mode water, AAIW = Antarctic intermediate water, and CPDW = circumpolar deep water (Sloyan et al., 2010). SAF = Sub-Antarctic Front, PF = Polar Front, and South ACC Front at 103°W (Figure S8; Park et al., 2019).

surface nutrient concentrations or the depth of nutricline (here presented as $Z_{nitrate}$ > 1 μM) had the strongest relationship with POM ratios. This supports the hypothesis that nutrient limitation is a primary driver for latitudinal shifts in C:N:P overall. However, the relative strength of the correlations between C:N:P and either nutrients or temperature varied regionally (Figure S6). After nutrients, temperature was the next best predictor of C:N:P, in particular within the Southern Ocean (Figure S6).

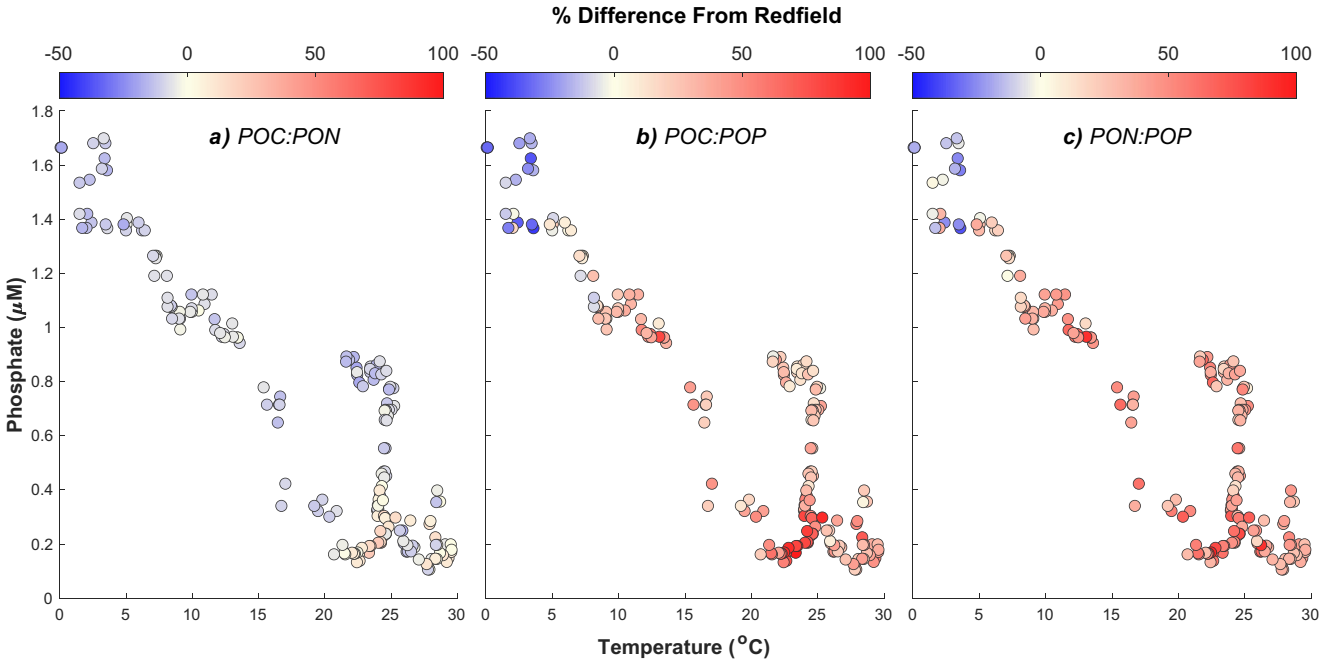

Figure 6. Environmental regulation of C:N:P stoichiometry. Relationship between surface phosphate (μM), temperature (°C) and (a) C:N, (b) C:P, and (c) N:P. Markers are colored based on percent difference from Redfield values (106C:16N:1P).

The relationship between environmental variation and C:N:P was more complex than previously appreciated (Figure 6). Phosphate concentration was used as a representative for macronutrient availability due to (i) a high correlation between surface nitrate and phosphate ($R^2 = 0.98$), (ii) phosphate is a more conservative tracer than nitrate (i.e., the marine phosphorus cycle is less complex than nitrogen) and is more commonly utilized in stoichiometric models, and (iii) nitrate was below detection limits in large parts of SPgyre. Decreasing temperature and increasing phosphate concentration both display a strong correlation to decreasing POM ratios south of 30°S (Figure S7). However, in locations of similar elevated temperature but variable phosphate concentration, C:N:P ratios were significantly different (Figures S7a–S7c, ANOVA p-values $< 1 \times 10^{-4}$). For areas with similar phosphate concentrations (e.g., $\left[PO_4\right]^{3-} = 0.95 \pm 0.15$ μM), but variable temperature, only N:P ratios showed significant differences (Figures S7d–S7f, ANOVA p-value = 0.003). We also observed that in areas of warm temperature (SST > 20°C) and low phosphate concentrations ($\left[PO_4\right]^{3-} = 0.2 \pm 0.1$ μM), regions can have significantly different POM ratios that cannot be attributed to either phosphate or temperature (Figures S7g–S7i). While nutrient availability appeared to the first-order driver of stoichiometric variability, we still observed large changes in C:N:P that cannot easily be attributed to known environmental drivers.

3.5. Deviations from Existing Stoichiometric Models

Despite regional correlation among environmental predictors and POM ratios, common models struggled in predicting the observed latitudinal variation in elemental stoichiometry within the eastern Pacific Ocean. The models included nutrient-dependence (Galbraith & Martiny, 2015), temperature-dependence (Yvon-Durocher et al., 2015), and a trait model (only for C:P, Moreno et al., 2018) (Figure 7). Both the temperature and single-nutrient (here nitrate) models systematically overestimated C:N for most of the transect and the temperature model showed the highest residual (Figure 7). It is important to note that we applied a lower detection limit of 0.1 μM, whereas the true nitrate concentration in surface low latitude waters is likely much lower. The temperature model also systematically overestimated C:P and N:P in most regions. This model had a strong positive residual in warm NPgyre waters, but matched observations in SOcean. A single-nutrient model based on phosphate showed less residual but struggled in capturing the gradient in C:P and N:P across the nutrient replete SOcean. None of the commonly applied models showed strong skill

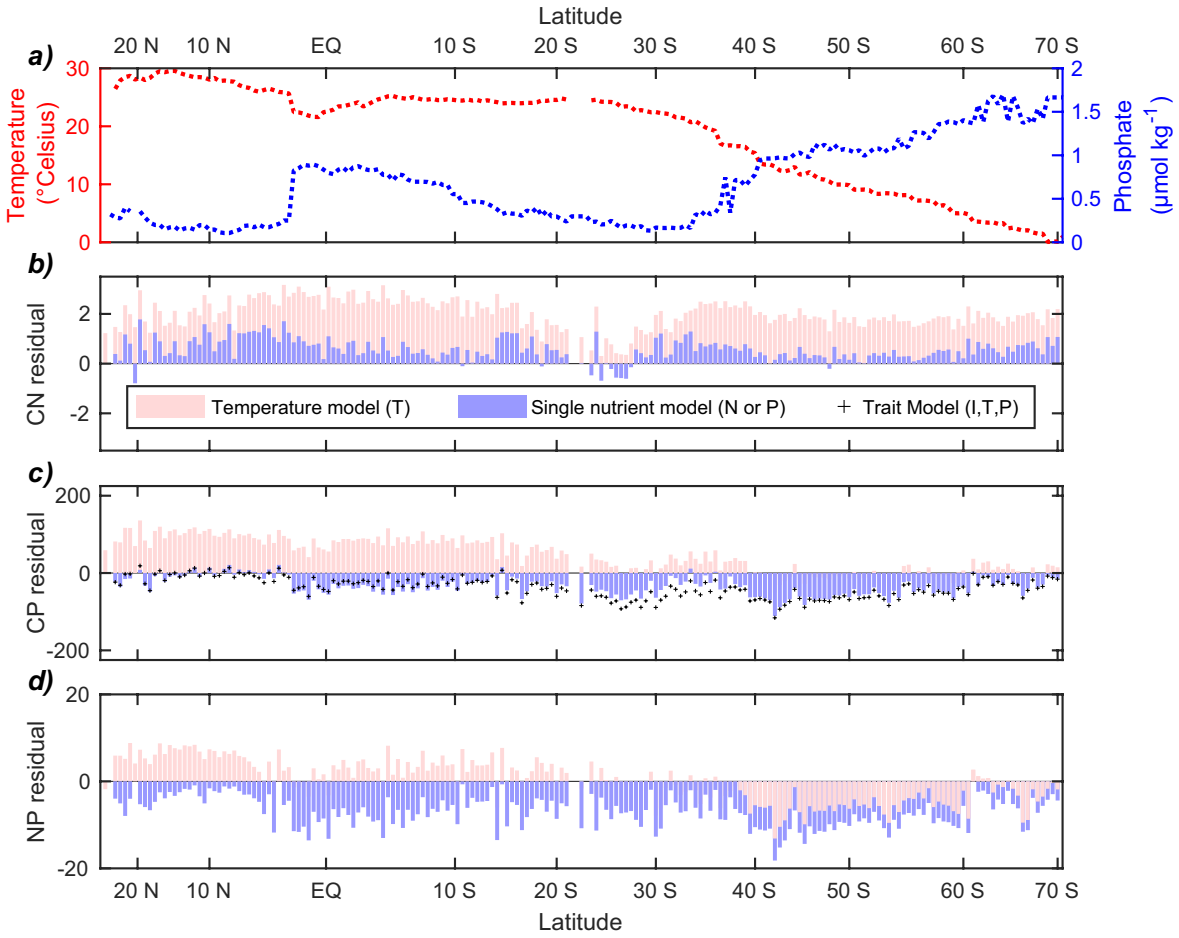

Figure 7. Stoichiometric model residuals for C:N, C:P, and N:P predictions. Observational inputs to stoichiometric models are plotted in (a) for temperature (red) and phosphate (blue) near 5 m depth. Residuals are calculated as predicted ratios—observations for (b) C:N, (c) C:P, and (d) N:P ratios. Positive values overestimate ratios, and vice versa for negative residuals. Stochiometric models used are a temperature regression model for C:P and N:P, a global regression model on phosphate (C:P) and nitrate (C:N), and a phytoplankton trait model for C:P. Each is described in the methods section. I = photosynthetically active radiation. T = temperature. P = phosphate.

in describing the latitudinal shift in C:N:P observed here, though locally fit models consistently improved skill relative to globally fit models (Table S6). Consequently, the nutrient (temperature) models tended to under (over)-predict the nutrient content of POM relative to C.

4. Discussion

4.1. Variable POM Stoichiometry

Our results validate past evidence of a latitudinal gradient in particulate organic matter ratios (Martiny, Pham, et al., 2013; Martiny, Vrugt, et al., 2013) but also suggest additional gradients in C:N:P within subtropical and polar biomes. Unlike compilation studies, an advantage to our study is that we target representative oceanic biomes in a single transect with consistent methodology. C:N:P ratios were higher than mean proportions (135 ± 29:22 ± 4:1) in the nutrient-poor gyres, but depressed in the Southern Ocean. Whereas C:P and N:P ratios were significantly higher than the expected Redfield proportions (106:16:1) in the nutrient-poor gyres, C:N and C:P ratios were significantly depressed in the nutrient-rich Southern Ocean. We were able to partially explain subtle shifts in C:N:P by previously proposed environmental drivers, but ultimately neither temperature, a single nutrient, or a trait-based model fully captured stoichiometry trends across the biomes. Accumulating evidence suggests that nutrient supply followed secondarily by temperature regulates POM stoichiometry (Garcia, Baer, et al., 2018; Garcia et al., 2020). In support, the temperature

model matches observed C:N:P in the Southern Ocean, but shows positive residuals for most of the eastern Pacific Ocean. Under the nutrient-supply hypothesis, elevated C:N and C:P ratios may be linked to N and P limitation, respectively (Klausmeier et al., 2004). Similar to Martiny, Vrugt, et al. (2013), we find lower C:N ratios in the North compared to south Pacific oligotrophic gyres (Figure 3a). However, an elevated C:P in the South Pacific gyre was inconsistent with the high observed phosphate concentrations (Galbraith & Martiny, 2015), and no current model can explain this gyre difference. The trait-based and single-nutrient models both assume luxury-P storage as a linear function of P, but recent studies propose a more complex storage response to phosphate supply rates (Cáceres et al., 2019; Garcia et al., 2020; Martin et al., 2014). Furthermore, cells may be unable to upregulate nutrient uptake transporters under severe N limitation (Bonachela et al., 2013), further restricting P quotas—something that is not captured in most current stoichiometry models. It is important to note that we used surface nitrate and phosphate concentrations as a proxy for nutrient availability. However, they may not capture changes in flux rates that also can impact elemental ratios. Another issue is the technical issue with measuring nitrate at low concentrations. Thus, we may not fully capture shifts in N availability over the P18 transect. The physical transport of low oxygen waters (denitrification and anammox conditions), as well as poor conditions for N_2-fixation, do still suggest N limitation in the SP gyre (Bonnet et al., 2008). Consequently, we need to develop models describing the interactions of multiple nutrients to describe the full variation of C:N:P.

4.2. Southern Ocean Ratios

Our data show that the latitudinal gradient in C:P and N:P within the Southern Ocean is linked to temperature and plankton community composition. Despite very high nutrient availability, we detected continually decreasing ratios southwards indicating a non-nutrient control on POM stoichiometry in SOcean. The temperature model provided a good fit to the N:P or C:P gradient raising the possibility that plankton in colder SOcean regions require a higher ribosome count to sustain growth (Toseland et al., 2013). We also measured allometric differences with lower ratios in larger particles. The N:P ratios observed in larger particles (~5–10) are similar to N:P cell quotas measured in polar diatoms (Lomas et al., 2019). As silicate concentrations were high and diatoms are known to dominate waters south of the Polar Frontal Zone, these observations lend support to the idea that growth of cold-water diatoms suppress N:P and C:P (Arrigo et al., 1999; Garcia, Sexton, et al., 2018; Weber & Deutsch, 2010). However, we also detected declining ratios in the small size fraction suggesting that smaller plankton show at least partially a similar response to temperature shifts. Thus, a combination of community shifts and temperature may control the observed stoichiometric gradient in the Southern Ocean.

4.3. Broader Impact of Dynamic Biogeochemical Processes

Surface particulate elemental ratios systematically deviate from constant proportions across the eastern Pacific Ocean with implications for biological processes including the regulation of primary productivity and the biological pump (Emerson et al., 2001; Schneider et al., 2004; Teng et al., 2014). The flexible stoichiometric ratios observed in marine communities (Martiny, Pham, et al., 2013; Martiny, Vrugt, et al., 2013) may provide an "export" buffer against stratification and lower surface ocean nutrient supply (Tanioka & Matsumoto, 2017). Our results indicate that large plankton populations contribute to lowering the C:N:P ratios in the Southern Ocean. To what extent the diversity of larger phytoplankton impacts the variability of organic matter remineralization in the deep thermocline remains an important question for modeling nutrient recycling and export in the Southern Ocean (Lomas et al., 2019; Moore et al., 2018; Weber & Deutsch, 2010). Our estimates of expected exported POM N:P according to N* values are closest to the observed values of the larger POM size fraction in SOcean. This suggests an increased contribution to exported POM from larger phytoplankton and/or aggregates in this region. Global biogeochemical models suggest incorporating a diverse plankton community and acclimation to multiple nutrients would more accurately represent spatial biogeochemical gradients (Buchanan et al., 2018; Fu et al., 2016; Tréguer et al., 2018). However, introducing additional complexity remains a real challenge. By assuming balanced growth at equilibrium, trait models can bridge this gap using an "instantaneous" biological response instead of a fully dynamic model (Ward, 2017). Temperature-based models with changing C:P will (with global warming) impact future biological carbon sequestration and oxygen declines. Nutrient-based models have similarly big

impacts for simulated changes in biogeochemical processes under enhanced overturning (and thus nutrient returns to the surface) from higher wind stresses or reduced overturning from enhanced stratification (from warming and freshwater additions). In the context of global environmental change, POM C:N:P ratios can help evaluate how and where changing temperatures, nutrient availability, and community structure will impact biogeochemical cycling.

Ultimately, various size classes of phytoplankton respond uniquely to environmental pressures and may contribute differentially to organic matter export. Similar to a recent meta-analysis of large and small phytoplankton C:N:P ratios and their environmental drivers (N, P, temp, light), we predict a high-light, warm and nutrient depleted system will produce higher proportions of C per P/N atom (Tanioka & Matsumoto, 2020). However, in contrast we find smaller POM C:N:P is more responsive to nutrient concentration and larger POM C:N:P to temperature (Table S7). While we primarily focus our discussion of exported POM on the larger size class examined in the Southern Ocean (Section 4.3), the contribution of smaller size classes to exported POM is unknown. While it is commonly assumed POM less than 20 μm (pico- and nano-plankton) contributes insignificantly, quantitative estimates of exported small POM vary widely among studies (Richardson, 2019). Alternative export pathways such as aggregation (Cruz & Neuer, 2019) or fecal pellets (Bisson et al., 2020) may be increasingly important as smaller phytoplankton are predicted to increase in abundance with increased warming and stratification (Flombaum et al., 2013; Moran, 2015). A recent study estimates nearly 60% of exported POM derives from zooplankton fecal pellets composed of small phytoplankton (Bisson et al., 2020). Given this uncertainty, understanding the connectivity between C:N:P in particles suspended in the euphotic zone versus sinking particles exported to depth is an important question.

Data Availability Statement

Hydrographic nutrient and CTD data collected aboard the P18 cruise line is available at https://cchdo.ucsd.edu/ Underway sea surface temperature from the NOAA R/V Ronald Brown is available at https://www.nodc.noaa.gov/tsg/ Particulate organic matter concentrations are available at BCO-DMO (http://doi.org/10.26008/1912/bco-dmo.816347.1). Photosynthetically active radiation was accessed from oceancolor.gsfc.nasa.gov (NASA Goddard Space Flight Center, Ocean Ecology Laboratory, Ocean Biology Processing Group. Moderate-resolution Imaging Spectroradiometer (MODIS) Aqua Photosynthetically Available Radiation Data; 2018 Reprocessing. NASA OB. DAAC, Greenbelt, MD, USA. http://doi.org/10.5067/AQUA/MODIS/L3B/PAR/2018).

Acknowledgments
We thank the captain and crew of the R/V Ronald H. Brown, the chief and co-chief scientists (Rolf Sonnerup, Annie Bourbonnais, and Sarah Purkey) and the science party on board the P18 cruise. The PMEL contribution number is 5083 and the JISAO contribution number is 2020–1059. In particular, we thank Eric Wisegarver and Charles Fischer for nutrient analysis. We also thank GO-SHIP coordinators Lynne Talley and Greg Johnson for their support. Funding for this study was provided by the National Science Foundation (OCE-1559002 and OCE-1848576) and the National Aeronautics and Space Administration Earth and Space Science Fellowship NESSF16 R to C.A.G. B.R.C. is grateful to Kathy Tedesco of the Global Ocean Monitoring and Observing division of NOAA for chief scientist funding through the NOAA GO-SHIP grant (U8R1SE3-PRF) and to NSF (OCE- 1437015) for also supporting the GO-SHIP program.

References

Arrigo, K. R. (2005). Marine microorganisms and global nutrient cycles. *Nature*, *437*(September), 349–355. https://doi.org/10.1038/nature04159

Arrigo, K. R., Robinson, D. H., Worthen, D. L., Dunbar, R. B., DiTullio, G. R., VanWoert, M., & Lizotte, M. P. (1999). Phytoplankton community structure and the drawdown of nutrients and CO2 in the Southern Ocean. *Science*, *283*(5400), 365–367. https://doi.org/10.1126/science.283.5400.365

Baer, S. E., Lomas, M. W., Terpis, K. X., Mouginot, C., & Martiny, A. C. (2017). Stoichiometry of Prochlorococcus, Synechococcus, and small eukaryotic populations in the western North Atlantic Ocean. *Environmental Microbiology*, *19*(4), 1568–1583. https://doi.org/10.1111/1462-2920.13672

Berman-Frank, I., Cullen, J. T., Shaked, Y., Sherrell, R. M., & Falkowski, P. G. (2001). Iron availability, cellular iron quotas, and nitrogen fixation in *Trichodesmium*. *Limnology & Oceanography*, *46*(6), 1249–1260. https://doi.org/10.4319/lo.2001.46.6.1249

Bisson, K., Siegel, D. A., & DeVries, T. (2020). Diagnosing mechanisms of ocean carbon export in a satellite-based food web model. *Frontiers in Marine Science*, *7*, 505. https://doi.org/10.3389/fmars.2020.00505

Bonachela, J. A., Allison, S. D., Martiny, A. C., & Levin, S. A. (2013). A model for variable phytoplankton stoichiometry based on cell protein regulation. *Biogeosciences*, *10*(6), 4341–4356. https://doi.org/10.5194/bg-10-4341-2013

Bonnet, S., Guieu, C., Bruyant, F., Prášil, O., Van Wambeke, F., Raimbault, P., et al. (2008). Nutrient limitation of primary productivity in the Southeast Pacific (BIOSOPE cruise). *Biogeosciences*. https://doi.org/10.5194/bg-5-215-2008

Buchanan, P. J., Matear, R. J., Chase, Z., Phipps, S. J., & Bindoff, N. L. (2018). Dynamic biological functioning important for simulating and stabilizing ocean biogeochemistry. *Global Biogeochemical Cycles*, *32*(4), 565–593. https://doi.org/10.1002/2017gb005753

Cáceres, C., Spatharis, S., Kaiserli, E., Smeti, E., Flowers, H., & Bonachela, J. A. (2019). Temporal phosphate gradients reveal diverse acclimation responses in phytoplankton phosphate uptake. *The ISME Journal*, *13*(11), 2834–2845. https://doi.org/10.1038/s41396-019-0473-1

Cruz, B. N., & Neuer, S. (2019). Heterotrophic Bacteria enhance the aggregation of the marine picocyanobacteria prochlorococcus and synechococcus. *Frontiers in Microbiology*, *10*(AUG), 1864. https://doi.org/10.3389/fmicb.2019.01864

Devries, T., & Deutsch, C. (2014). Large-scale variations in the stoichiometry of marine organic matter respiration. *Nature Geoscience*, *7*(12), 890–894. https://doi.org/10.1038/ngeo2300

Ducklow, H., & Dickson, A. (1994). *Shipboard sampling procedures* (pp. 1–210). Jgofs.

Emerson, S., Mecking, S., & Abell, J. (2001). The biological pump in the subtropical North Pacific Ocean: Nutrient sources, Redfield ratios, and recent changes. *Global Biogeochemical Cycles*, *15*(3), 535–554. https://doi.org/10.1029/2000gb001320

Escribano, R., Daneri, G., Farías, L., Gallardo, V. A., González, H. E., Gutiérrez, D., et al. (2004). Biological and chemical consequences of the 1997-1998 El Niño in the Chilean coastal upwelling system: A synthesis. In *Deep-sea research Part II: Topical studies in Oceanography*. https://doi.org/10.1016/j.dsr2.2004.08.011

Fay, A. R., & McKinley, G. A. (2014). Global open-ocean biomes: Mean and temporal variability. *Earth System Science Data*, *6*(2), 273–284. https://doi.org/10.5194/essd-6-273-2014

Finkel, Z. V., Follows, M. J., Liefer, J. D., Brown, C. M., Benner, I., & Irwin, A. J. (2016). Phylogenetic diversity in the macromolecular composition of microalgae. *PloS One*, *11*(5), e0155977. https://doi.org/10.1371/journal.pone.0155977

Flombaum, P., Gallegos, J. L., Gordillo, R. A., Rincon, J., Zabala, L. L., Jiao, N., et al. (2013). Present and future global distributions of the marine Cyanobacteria Prochlorococcus and Synechococcus. *Proceedings of the National Academy of Sciences*, *110*(24), 9824–9829. https://doi.org/10.1073/pnas.1307701110

Fu, W., Randerson, J. T., & Moore, J. K. (2016). Climate change impacts on net primary production (NPP) and export production (EP) regulated by increasing stratification and phytoplankton community structure in the CMIP5 models. *Biogeosciences*, *13*, 5151–5170. https://doi.org/10.5194/bg-13-5151-2016

Galbraith, E. D., & Martiny, A. C. (2015). A simple nutrient-dependence mechanism for predicting the stoichiometry of marine ecosystems. *Proceedings of the National Academy of Sciences of the United States of America*, *112*(27), 8199–8204. https://doi.org/10.1073/pnas.1423917112

Garcia, C. A., Baer, S. E., Garcia, N. S., Rauschenberg, S., Twining, B. S., Lomas, M. W., & Martiny, A. C. (2018). Nutrient supply controls particulate elemental concentrations and ratios in the low latitude eastern Indian Ocean. *Nature Communications*, *9*(1), 4868. https://doi.org/10.1038/s41467-018-06892-w

Garcia, C. A., Hagstrom, G. I., Larkin, A. A., Ustick, L. J., Levin, S. A., Lomas, M. W., & Martiny, A. C. (2020). Linking regional shifts in microbial genome adaptation with surface ocean biogeochemistry. *Philosophical Transactions of the Royal Society B*, *375*, 20190254. https://doi.org/10.1098/rstb.2019.0254

Garcia, N. S., Sexton, J., Riggins, T., Brown, J., Lomas, M. W., & Martiny, A. C. (2018). High variability in cellular stoichiometry of carbon, nitrogen, and phosphorus within classes of marine eukaryotic phytoplankton under sufficient nutrient conditions. *Frontiers in Microbiology*. https://doi.org/10.3389/fmicb.2018.00543

Geider, R. J., & La Roche, J. (2002). Redfield revisited: Variability of C:N:P in marine microalgae and its biochemical basis. *European Journal of Phycology*. https://doi.org/10.1017/S0967026201003456

Hein, M., Pedersen, M., & Sand-Jensen, K. (1995). Size-dependent nitrogen uptake in micro- and macroalgae. *Marine Ecology Progress Series*, *118*, 247–253. https://doi.org/10.3354/meps118247

Huffman, G. J., Stocker, E. F., Bolvin, D. T., Nelkin, E. J., & Tan, J. (2019). *GPM IMERG final precipitation L3 1 month 0.1 degree x 0.1 degree V06*. Goddard Earth Sciences Data and Information Services Center (GES DISC). https://doi.org/10.5067/GPM/IMERG/3B-MONTH/06

Kalnay, E., Kanamitsu, M., Kistler, R., Collins, W., Deaven, D., Gandin, L., et al. (1996). The NCEP/NCAR 40-Year Reanalysis Project. *Bulletin of the American Meteorological Society*, *77*(3), 437–471. https://doi.org/10.1175/1520-0477(1996)077<0437:tnyrp>2.0.co;2

Klausmeier, C. A., Litchman, E., & Levin, S. A. (2004). Phytoplankton growth and stoichiometry under multiple nutrient limitation. *Limnology & Oceanography*, *49*, 1463–1470. https://doi.org/10.4319/lo.2004.49.4_part_2.1463

Lauvset, S. K., Key, R. M., Olsen, A., van Heuven, S., Velo, A., Lin, X., et al. (2016). A new global interior ocean mapped climatology: The 1° × 1° GLODAP version 2. *Earth System Science Data*, *8*(2), 325–340. https://doi.org/10.5194/essd-8-325-2016

Lomas, M. W., Baer, S. E., Acton, S., & Krause, J. W. (2019). Pumped up by the cold: Elemental quotas and stoichiometry of cold-water diatoms. *Frontiers in Marine Science*. https://doi.org/10.3389/fmars.2019.00286

Lomas, M. W., Burke, A. L., Lomas, D. A., Bell, D. W., Shen, C., Dyhrman, S. T., & Ammerman, J. W. (2010). Sargasso Sea phosphorus biogeochemistry: An important role for dissolved organic phosphorus (DOP). *Biogeosciences*, *7*(2), 695–710. https://doi.org/10.5194/bg-7-695-2010

Martin, P., Dyhrman, S. T., Lomas, M. W., Poulton, N. J., & Van Mooy, B. A. S. (2014). Accumulation and enhanced cycling of polyphosphate by Sargasso Sea plankton in response to low phosphorus. *Proceedings of the National Academy of Sciences*, *111*(22), 8089–8094. https://doi.org/10.1073/pnas.1321719111

Martiny, A. C., Pham, C. T. A., Primeau, F. W., Vrugt, J. A., Moore, J. K., Levin, S. A., & Lomas, M. W. (2013). Strong latitudinal patterns in the elemental ratios of marine plankton and organic matter. *Nature Geoscience*, *6*(4), 279–283. https://doi.org/10.1038/ngeo1757

Martiny, A. C., Vrugt, J. A., Primeau, F. W., & Lomas, M. W. (2013). Regional variation in the particulate organic carbon to nitrogen ratio in the surface ocean. *Global Biogeochemical Cycles*, *27*(3), 723–731. https://doi.org/10.1002/gbc.20061

Mills, M. M., & Arrigo, K. R. (2010). Magnitude of oceanic nitrogen fixation influenced by the nutrient uptake ratio of phytoplankton. *Nature Geoscience*, *3*(6), 412–416. https://doi.org/10.1038/ngeo856

Moore, J. K., Fu, W., Primeau, F., Britten, G. L., Lindsay, K., Long, M., et al. (2018). Sustained climate warming drives declining marine biological productivity. *Science*, *359*(6380), 113–1143. https://doi.org/10.1126/science.aao6379

Moran, M. A. (2015). The global ocean microbiome. *Science*. https://doi.org/10.1126/science.aac8455

Mordy, C., Zhang, J.-Z., Sigman, D., Johnson, G., & Baringer, M. (2017). *CTD and Bottle data from cruise 33RO20161119, exchange version*. CCHDO cruise. https://doi.org/10.7942/C21T0F

Moreno, A. R., Hagstrom, G. I., Primeau, F. W., Levin, S. A., & Martiny, A. C. (2018). Marine phytoplankton stoichiometry mediates nonlinear interactions between nutrient supply, temperature, and atmospheric CO_2. *Biogeosciences*, *15*(9), 2761–2779. https://doi.org/10.5194/bg-15-2761-2018

Moreno, A. R., & Martiny, A. C. (2018). Ecological Stoichiometry of Ocean Plankton. *Annual Review of Marine Science*, *10*(August), 1–27. https://doi.org/10.1146/annurev-marine-121916-063126

Orsi, A. H., Whitworth, T., & Nowlin, W. D. (1995). On the meridional extent and fronts of the Antarctic Circumpolar Current. *Deep Sea Research Part I: Oceanographic Research Papers*, *42*(5), 641–673. https://doi.org/10.1016/0967-0637(95)00021-w

Pahlow, M., & Oschlies, A. (2009). Chain model of phytoplankton P, N and light colimitation. *Marine Ecology Progress Series*, *376*, 69–83. https://doi.org/10.3354/meps07748

Park, Y. H., Park, T., Kim, T. W., Lee, S. H., Hong, C. S., Lee, J. H., et al. (2019). Observations of the Antarctic Circumpolar Current over the Udintsev Fracture Zone, the Narrowest Choke Point in the Southern Ocean. *Journal of Geophysical Research: Oceans*, *124*(7), 4511–4528. https://doi.org/10.1029/2019jc015024

Price, N. M. (2005). The elemental stoichiometry and composition of an iron-limited diatom. *Limnology & Oceanography*, *50*(4), 1159–1171. https://doi.org/10.4319/lo.2005.50.4.1159

Redfield, A. C. (1934). *On the proportions of organic derivatives in sea water and their relation to the composition of plankton* (James Johnstone Memorial Volume, pp. 176–192). University Press of Liverpool.

Reygondeau, G., Longhurst, A., Martinez, E., Beaugrand, G., Antoine, D., & Maury, O. (2013). Dynamic biogeochemical provinces in the global ocean. *Global Biogeochemical Cycles*, *27*(4), 1046–1058. https://doi.org/10.1002/gbc.20089

Richardson, T. L. (2019). Mechanisms and pathways of small-phytoplankton export from the Surface Ocean. *Annual Review of Marine Science*, *11*(1), 57–74. https://doi.org/10.1146/annurev-marine-121916-063627

Schneider, B., Engel, A., & Schlitzer, R. (2004). Effects of depth- and CO2-dependent C:N ratios of particulate organic matter (POM) on the marine carbon cycle. *Global Biogeochemical Cycles*, *18*(2). https://doi.org/10.1029/2003gb002184

Sloyan, B. M., Talley, L. D., Chereskin, T. K., Fine, R., & Holte, J. (2010). Antarctic intermediate water and sub Antarctic mode water formation in the Southeast Pacific: The role of turbulent mixing. *Journal of Physical Oceanography*, *40*(7), 1558–1574. https://doi.org/10.1175/2010jpo4114.1

Smith, R. E. H., & Kalff, J. (1982). Size-dependent phosphorus uptake kinetics and cell quota in phytoplankton. *Journal of Phycology*, *18*(2), 275–284. https://doi.org/10.1111/j.1529-8817.1982.tb03184.x

Solórzano, L., & Sharp, J. H. (1980). Determination of total dissolved phosphorus and particulate phosphorus in natural waters? *Limnology & Oceanography*, *25*, 754–758. https://doi.org/10.4319/lo.1980.25.4.0754

Tanioka, T., & Matsumoto, K. (2017). Buffering of ocean export production by flexible elemental stoichiometry of particulate organic matter. *Global Biogeochemical Cycles*, *31*(10), 1528–1542. https://doi.org/10.1002/2017gb005670

Tanioka, T., & Matsumoto, K. (2020). A meta-analysis on environmental drivers of marine phytoplankton C:N:P. *Biogeosciences*, *17*(11), 2939–2954. https://doi.org/10.5194/bg-17-2939-2020

Teng, Y.-C., Primeau, F. W., Moore, J. K., Lomas, M. W., & Martiny, A. C. (2014). Global-scale variations of the ratios of carbon to phosphorus in exported marine organic matter. *Nature Geoscience*, *7*(12), 895–898. https://doi.org/10.1038/ngeo2303

Toseland, A., Daines, S. J., Clark, J. R., Kirkham, A., Strauss, J., Uhlig, C., et al. (2013). The impact of temperature on marine phytoplankton resource allocation and metabolism. *Nature Climate Change*, *3*(11), 979–984. https://doi.org/10.1038/nclimate1989

Tréguer, P., Bowler, C., Moriceau, B., Dutkiewicz, S., Gehlen, M., Aumont, O., et al. (2018). Influence of diatom diversity on the ocean biological carbon pump. *Nature Geoscience*. https://doi.org/10.1038/s41561-017-0028-x

Ward, B. A. (2017). Assessing an efficient "Instant Acclimation" approximation of dynamic phytoplankton stoichiometry. *Journal of Plankton Research*, *39*(5), 803–814. https://doi.org/10.1093/plankt/fbx040

Weber, T. S., & Deutsch, C. (2010). Ocean nutrient ratios governed by plankton biogeography. *Nature*, *467*. https://doi.org/10.1038/nature09403

Yvon-Durocher, G., Dossena, M., Trimmer, M., Woodward, G., & Allen, A. P. (2015). Temperature and the biogeography of algal stoichiometry. *Global Ecology and Biogeography*, *24*(5), 562–570. https://doi.org/10.1111/geb.12280